Diesoline, Diesohol and Diesosene Fuelled HCCI Engine Development

Article *in* Journal of Energy Resources Technology, Transactions of the ASME · May 2016

DOI: 10.1115/1.4033571

2 authors:

Akhilendra Pratap Singh
Indian Institute of Technology Kanpur
102 PUBLICATIONS **3,569** CITATIONS

SEE PROFILE

Avinash Kumar Agarwal
Indian Institute of Technology Kanpur
580 PUBLICATIONS **23,048** CITATIONS

SEE PROFILE

Diesoline, Diesohol, and Diesosene Fuelled HCCI Engine Development

Akhilendra Pratap Singh
Engine Research Laboratory,
Department of Mechanical Engineering,
Indian Institute of Technology Kanpur,
Kanpur 208016, India
e-mail: akhips@iitk.ac.in

Avinash Kumar Agarwal[1]
Engine Research Laboratory,
Department of Mechanical Engineering,
Indian Institute of Technology Kanpur,
Kanpur 208016, India
e-mail: akag@iitk.ac.in

Compression ignition (CI) engines are facing strong restrictive emission norms globally, which demand extremely low oxides of nitrogen (NOx) and particulate matter (PM) emissions. Homogeneous charge compression ignition (HCCI) engine is a very attractive solution to meet these stringent emission challenges due to its capability to simultaneously reduce NOx and PM. In this study, HCCI combustion was investigated using different test fuels such as diesoline (15% v/v gasoline with diesel), diesohol (15% v/v ethanol with diesel), and diesosene (15% v/v kerosene with diesel) vis-a-vis baseline mineral diesel. A dedicated fuel vaporizer was used for homogeneous fuel–air mixture preparation. The experiments were performed at constant intake charge temperature (180 °C), fixed exhaust gas recirculation (EGR) (15%) at different engine loads. Stable combustion characteristics were determined for diesosene at lower engine loads, however, diesoline and diesohol yielded improved emissions compared to baseline diesel HCCI combustion. At higher loads, diesoline and diesosene showed higher knocking tendency compared to baseline diesel and diesohol. Diesohol showed lower NOx and smoke opacity, however, diesoline and diesosene showed slightly lower hydrocarbon (HC) and carbon monoxide (CO) emissions compared to baseline diesel HCCI combustion. Performance results of diesohol and diesosene were slightly inferior compared to diesel and diesoline HCCI combustion. Physical characterization of exhaust particulates was done for these test fuels using engine exhaust particle sizer (EEPS). Particle number-size distribution showed that most particles emitted from diesoline and diesohol were in ultrafine size range and baseline diesel and diesosene emitted relatively larger particles. Reduction in total particle number concentration with addition of volatile fuel components in mineral diesel was another important observation of this study. [DOI: 10.1115/1.4033571]

Introduction

Automotive industry is required to develop cleaner technologies with lower fuel consumption for ambient air quality improvement, greenhouse gas reduction, and energy security. It is well known that the availability of conventional engine fuels is depleting rapidly. Due to continuously evolving stringent emission norms, as well as dwindling primary energy sources, development of new, efficient, and environment-friendly combustion systems fuelled by alternative fuels has become important.

HCCI is considered as an alternative engine combustion concept. HCCI combustion is an advanced concept with benefits of simultaneously reducing NOx and PM, while achieving higher thermal efficiency and capability of using multitude of fuels such as mineral diesel, gasoline, and biofuels (alcohols, biodiesel, etc.) [1–3]. In HCCI engines, combustion occurs because of spontaneous auto-ignition at multiple locations throughout the cylinder. A homogeneous air–fuel mixture is inducted/generated during the intake stroke and toward the compression stroke it attains auto-ignition conditions and combusts spontaneously, precisely at the end of the compression stroke/beginning of the expansion stroke. A large number of researchers have already demonstrated this new volumetric combustion concept using appropriate optical diagnostics [4,5]. Volumetric combustion in HCCI is attributed by homogeneous fuel–air mixing, which improves emission characteristics, i.e., it reduced NOx and PM simultaneously. HCCI combustion, however, suffers from the lack of direct ignition control and high rate of pressure rise (RoPR), which occurs during premixed combustion, thus, making it unsuitable for high engine loads [1,2,4–6].

HCCI technique was first discovered by Onishi et al. on a gasoline-fueled engine [7]. Najt and Foster [8] focused on developing detailed mechanism of HCCI combustion. In the experiments, they observed two distinct stages during HCCI combustion, in which first one was due to low temperature chemistry (below 1000 K) and the second one was due to high temperature chemistry (above 1000 K). Auto-ignition of homogeneous fuel–air mixture was controlled by low temperature chemistry however bulk heat release during combustion was controlled by high temperature chemistry. HCCI combustion of diesel-like fuels was challenging for researchers because low volatility of diesel limits homogeneous fuel–air mixing and charge preparation [9]. For diesel HCCI, three techniques namely port fuel injection with preheated air, in-cylinder mixture preparation, and external mixture preparation were used by different research groups. Ryan and Callahan [10] injected diesel into the preheated intake air. In this technique, temperature of heated air led to another limitation due to significant cool-combustion chemistry of diesel. This resulted in rapid auto-ignition, once compression temperatures were above 800 K [10,11].

Use of external charge preparation device was another solution adopted by several researchers [1,6,12,13]. In this technique, fuel–air mixing was enhanced by two techniques namely fuel atomization and fuel vaporization. Shawn et al. [12] used a diesel atomizer to enhance fuel atomization, which resulted in significant improvement in fuel–air mixing. They attained HCCI combustion successfully and further investigated the effect of different operating parameters on HCCI combustion. Singh and Agarwal [1,6] developed a device named "fuel vaporizer" for evaporation of low volatility diesel-like fuels. They carried out diesel HCCI experiments to examine different control parameters and reported that EGR is the most promising solution to optimize combustion

[1]Corresponding author.

Contributed by the Internal Combustion Engine Division of ASME for publication in the JOURNAL OF ENERGY RESOURCES TECHNOLOGY. Manuscript received February 26, 2015; final manuscript received April 25, 2016; published online June 14, 2016. Assoc. Editor: Stephen A. Ciatti.

phasing. EGR reduced combustion temperature and diluted the charge, which in turn delayed the start of combustion (SoC), resulting in lower maximum cylinder pressure.

Massive research efforts proved that HCCI combustion significantly lowers NOx emission, however, there were concern to reduce PM emission. Kittelson and Franklin [14] investigated the chemical characteristics of PM and found that diesel HCCI PM comprised of lesser solid, accumulation mode particles, and more volatile nuclei mode particles. They suggested that PM emission depends on two factors: soot formation during initial combustion and oxidation post combustion. Due to lower peak cylinder temperature, higher condensable PM fraction in HCCI mode results in higher particulate phase HC emissions. Agarwal et al. investigated emissions and particulate characteristics of diesel and gasoline-fuelled HCCI engine [15,16]. They reported improved emission characteristics and lesser particle number concentration for diesel HCCI combustion compared to conventional CI combustion.

Previous research studies related to combustion, performance, emission, and particle emission characteristics suggest that diesel HCCI combustion can be improved by increasing test fuel volatility. This can be achieved by addition of volatile additives/fuels to diesel-like fuels. Chao et al. [17] performed experiments using diesel–gasoline blends and reported relatively higher thermal efficiency in HCCI mode than gasoline spark ignition (SI) engines. Under optimum operating conditions, thermal efficiency was slightly higher than diesel engines. They also reported significant reduction in soot emission with increasing gasoline fraction in the test fuel. Han et al. [18] performed HCCI experiments using diesel–gasoline blends. Longer ignition delay and lower soot emission due to higher fuel volatility were the important findings of their research. Alcohols were suggested as another promising alternative fuel, which have potential to improve air quality by undergoing cleaner combustion [19,20]. Main advantage of alcohol blending with diesel was its oxygen content, which is 34% (w/w) for ethanol. Ethanol is the main alcohols considered to be a suitable alternative to gasoline and several researchers have investigated HCCI combustion characteristic using ethanol [21–23]. Presence of moisture traces in anhydrous ethanol reduces its solubility in mineral diesel and affects combustion [24]. Researchers have carried out experiment in CI engines using diesohol (mixture of alcohol with diesel) and reported significant and simultaneous reduction in PM and NOx emissions [25–27]. Ahmed [26] performed experiments in heavy-duty diesel engine using 10% ethanol blended with mineral diesel and reported 30–50% reduction in PM emission compared to low sulphur diesel. Gasoline and alcohols are therefore suitable additives for volatility improvement of mineral diesel.

Kerosene also has lower boiling range/temperature compared to mineral diesel and exhibits comparable combustion characteristics. Therefore, kerosene can be another possible option for volatility improvement of mineral diesel. Yadav et al. [28] measured the fuel properties of kerosene–diesel blend and found relatively lower kinematic viscosity and density of blends compared to baseline mineral diesel. Lower density and viscosity of kerosene compared to diesel make it suitable for fuel vaporizer application in HCCI. Due to the presence of lighter fractions in kerosene, fuel vaporizer's performance improves and superior fuel–air mixture could be possibly obtained. Pathak et al. [29] performed experiments on a genset SI engine using kerosene and developed methodology for optimization of fuel consumption, without adversely affecting engine performance parameters. Bergstrand [30] performed experiments on a conventional CI engine using mineral diesel and diesel–kerosene blends and compared their soot emission characteristics. They reported lower soot emissions from diesel–kerosene blends at lower engine loads. Lower cetane number of kerosene was the main reason for this trend, which was due to relatively longer ignition delay.

This research study is directed toward development of methodology for formation of homogeneous fuel–air mixture outside the combustion chamber. An electrically heated external fuel–air mixing device fuel vaporizer was used for homogeneous charge preparation. Various experiments were performed on the HCCI engine to investigate the combustion, performance, and emission characteristics at varying loads. Particle size-number distribution was measured to evaluate the particulate emission characteristics using modified fuels in HCCI mode. Three test fuels namely diesoline (15% v/v gasoline with diesel), diesohol (15% v/v ethanol with diesel), and diesosene (15% v/v kerosene with diesel) were used in this study, along with baseline mineral diesel.

Experimental Setup

The schematic of HCCI experimental setup is shown in Fig. 1.

Experiments were performed on a constant speed, two-cylinders, four-stroke, air-cooled, direct-injection diesel engine (Kirloskar, India; DA-16). One cylinder of the engine was modified to operate in HCCI mode, while the other cylinder operated in conventional CI combustion mode. Compression ratio of HCCI cylinder was reduced to 16.5. Test engine was coupled with a single phase 11 kW, 220 volt AC alternator. A 10 kW resistive load was connected to the AC alternator for loading the engine. Technical specifications of the original test engine, before the modifications, are given in Table 1.

Due to lower volatility of mineral diesel, homogeneous mixture preparation remains the most critical part of diesel HCCI experiments. In the present investigations, homogeneous charge was prepared by the fuel vaporizer. Schematic of the fuel vaporizer is shown in Fig. 2.

Main vaporizing chamber of the fuel vaporizer is made of aluminum cylinder (due to its high thermal conductivity and low reactivity). Cylindrical surface of this chamber was covered externally by a ceramic band heater, which provides necessary heating for fuel droplet vaporization. Temperature of electrical heater was controlled by a proportional integral differential (PID) temperature controller. The cut-off temperature for the temperature controller was $180 \pm 5\,^{\circ}C$. Specifications of the fuel vaporizer are given in Table 2.

Fuel was injected in the preheated main vaporizer chamber by a port fuel injector. This injector was connected to a fuel accumulator, which maintains 3 bar fuel pressure. Energy supplied by the heater is absorbed by atomized fuel spray droplets, and they eventually get converted into fuel vapor. High velocity air supplied from a blower forces fuel vapors to mix with the intake air and forms homogeneous charge. This homogeneous charge is then inducted into the combustion chamber via intake valve.

For controlling the port fuel injector, a dedicated injection driver circuit was designed, which controlled the injection parameters such as start of injection, injection delay, pulse duration, hence, injection quantity. It receives input for top dead center (TDC) and generates a trigger signal for the solenoid injector. In-cylinder pressure was measured using a piezoelectric pressure transducer, which was mounted flush into the cylinder head. For crank angle measurement, an angle encoder with a resolution 0.1 crank angle degree (CAD) was installed onto the engine crankshaft. For data acquisition and analysis, a high speed combustion data acquisition system (DAQ) (AVL, Austria; Indimicro) was used. This system acquires pressure signal as input and processes the data to deliver combustion and knocking parameters. Schematic of fuel injection and DAQ is shown in Fig. 3.

To control the rate of heat release (RoHR) and combustion phasing, a part of the exhaust gas was recirculated into the combustion chamber. A U-tube manometer was used to measure the flow rate of EGR across a calibrated orifice plate. Intake air supplied to HCCI cylinder was a mixture of fresh air from the surge tank, heated air–fuel mixture from the fuel vaporizer, and the recirculated exhaust gas. Flow rate of each stream was regulated and controlled by flow regulators. Several thermocouples were installed for measurement of exhaust gas temperature (EGT), intake charge temperature, and EGR temperature. Exhaust line of HCCI cylinder was separated from CI cylinder. Gaseous exhaust species

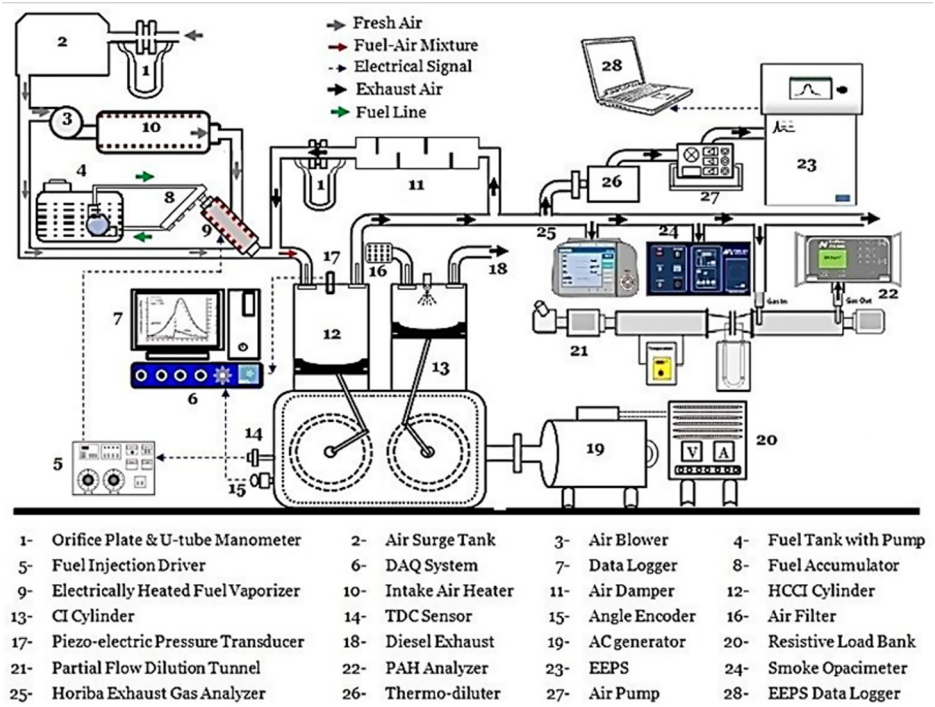

Fig. 1 HCCI experimental setup

Table 1 Original engine specifications

Characteristics	Specifications
Make/model/type	Kirloskar, DA16, diesel engine
Injection type	DI
Number of cylinders	Two
Bore/stroke	87.5/110 mm
Power output/cylinder	5.5 kW at 1500 rpm
Compression ratio	17.5:1
Displacement/cylinder	659 cc
Fuel injection timing (SOI)	24 deg before TDC
Fuel injection pressure	220 bar at 1500 rpm

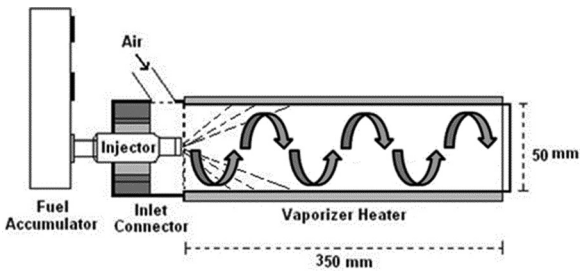

Fig. 2 Schematic of the fuel vaporizer

Table 2 Fuel vaporizer specifications

Characteristics	Specifications
Power supply to heater	1800 W
Vaporizer diameter	50 mm
Length of vaporizer	350 mm
Warm-up time	3 min
Cut-off temperature	180±5 °C
Diesel injection pressure	3.0 bar

were measured using portable exhaust gas analyzer (Horiba, Japan; MEXA584L), which gave raw emission concentrations of NO, HC, CO, O_2, and CO_2. Smoke opacity of the exhaust gas was measured by Smoke opacitymeter (AVL, Austria; 437). EEPS (TSI, USA; EEPS 3090) is a fast-response, high-resolution instrument. It can measure particles in a size range from 5.6 nm to 560 nm with a concentration of upto 10^8 particles/cc of exhaust. EEPS was used to measure particle size-number distribution in diluted exhaust. Polycyclic aromatic hydrocarbons (PAHs) in the engine exhaust were measured using an online PAH analyzer (Eco-Chem Labs, USA; PAS 2000). PAH analyzer works on the principle of photo-ionization of particle-bound PAH and conducts real time monitoring of particle bound PAH's.

The experiments were performed using blends of gasoline, ethanol, and kerosene with baseline mineral diesel. Important properties of base fuels are given in Table 3. Table 4 shows the important properties of test fuels used in HCCI experiments. Diesoline has lowest density and highest calorific value among all test fuels.

Figure 4 shows the volatile characteristics of test fuels. Results of fuel volatility showed that baseline mineral diesel has lowest volatility among the test fuels, however, diesoline has highest volatility among the test fuels. At low temperatures, volatility of test fuels showed significant difference however at higher temperatures, all fuels showed almost similar behavior. Effect of relatively higher volatility of gasoline can be observed in distillation curve of diesoline.

Results and Discussion

Experiments were performed at constant intake air temperature (180 °C), and fixed EGR (15%) at six different relative fuel–air ratios (λ). For fuel–air ratio calculation, injector calibration was performed for each test fuel. For injector calibration, fuel injection was done 12.5 Hz (equivalent to 1500 rpm engine speed) and fuel injected was collected at different injector pulse durations for 750 injections in 1 min. Each sample was weighted and results were plotted w.r.t. pulse duration to draw the calibration curve (Fig. 5). Calibration curves show a direct correlation between injector

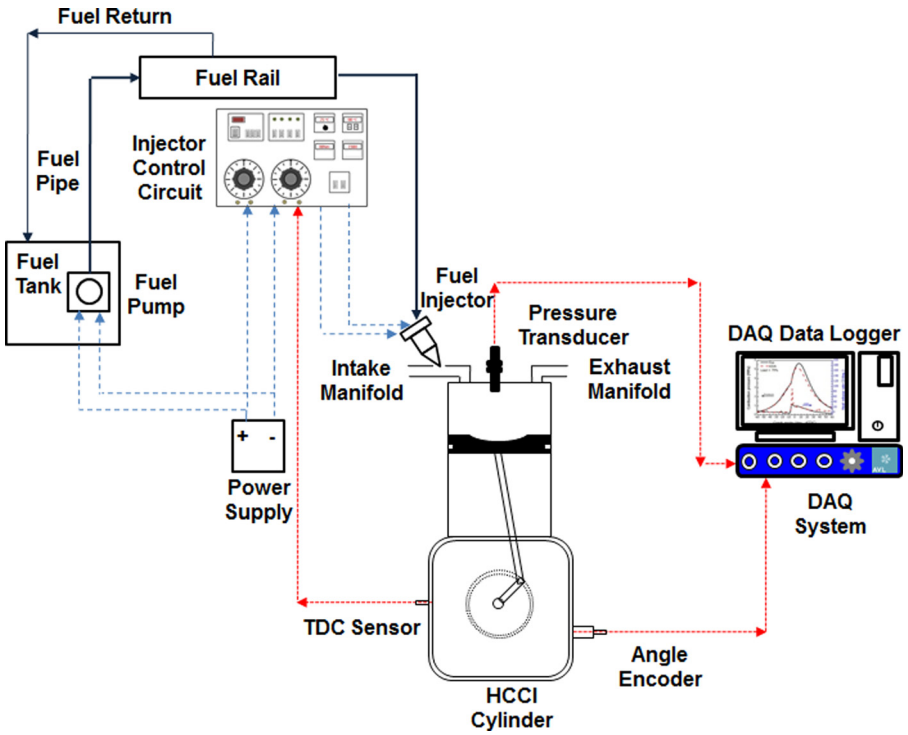

Fig. 3 Schematic of fuel injection and DAQ system

Table 3 Important properties of diesel, gasoline, ethanol, and kerosene

Properties	Diesel	Gasoline	Ethanol	Kerosene
Density (kg/m^3)	832	703	789	797
Viscosity at 40 °C (cS)	1–4	0.5–0.7	1–2	1.5–2.1
Cetane number	45–48	—	10	35–40
Calorific value (MJ/kg)	42.42	47.3	31.4	45.4
Flash point (°C)	55	−42	18	40–70
Auto-ignition temperature	250	280	380	230
Boiling temperature(°C)	160–330	30–200	80	145–280
Oxygen content (wt. %)	0	0	34.75	0
Average number of carbon	16–23	5–11	2	11–19

Table 4 Important properties of test fuels

Properties	Diesel	Diesoline	Diesohol	Diesosene
Density (kg/m^3)	832	794	804.3	807.5
Viscosity at 40 °C (cS)	2.78	1.98	2.42	2.27
Calorific value (MJ/kg)	42.42	43.23	38.9	42.89

performance and fuel properties. To avoid measurement errors, calibration was done thrice and the average of these was used.

Air flow rate to the engine was measured using calibrated orifice plate and U-tube manometer. Using these two parameters, air–fuel ratios (λ) were calculated for HCCI experiment. HCCI combustion was achieved in a wide range of λ (1.5–5.25). For $\lambda > 5.25$, HCCI combustion could not be achieved. Hence, $\lambda = 5.25$ was chosen as the lean limit (misfire limit) for these experiments. Similarly for mixtures richer than $\lambda = 1.5$, combustion was erratic and noisy due to severe knocking. Therefore, $\lambda = 1.5$ was chosen as the rich limit (knocking limit) for these experiments. Experiments were performed at six different engine loads (at six different values of λ), in which $\lambda = 1.5$ and 2.25 were taken as higher engine loads (indicated mean effective pressure (IMEP)$\sim$3.75 to 4.5 bar), $\lambda = 3.0$ and 3.75 were considered medium engine load (IMEP$\sim$3.0 to 4.0 bar), $\lambda = 4.5$ and 5.25 were considered as lower engine loads (IMEP $\sim$ 1.5 to 2.5 bar). Effect of λ on the combustion, performance, emission and particulate characteristics of HCCI engine is described in the next sections.

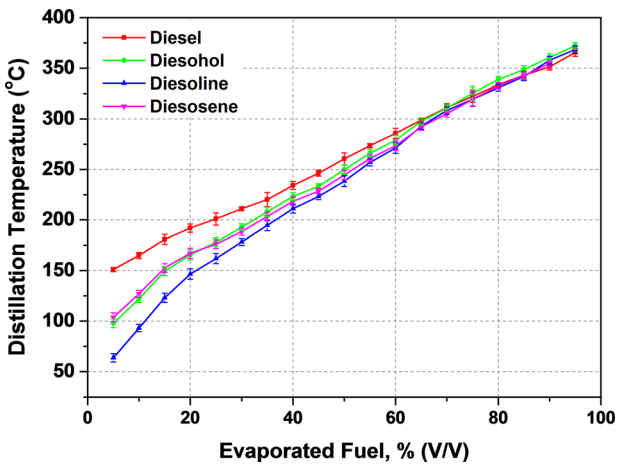

Fig. 4 Volatility characteristics of test fuels

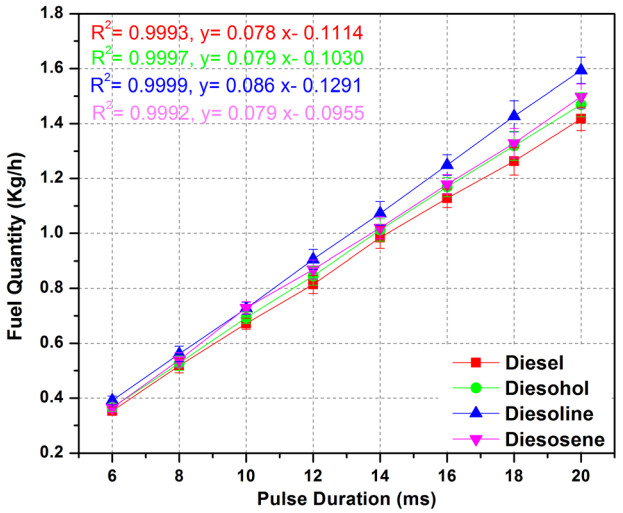

Fig. 5 Injector calibration curves for mineral diesel, diesohol, diesoline, and diesosene

Combustion Analysis. Combustion analysis is divided into following subsections, namely pressure-crank angle (P–θ) analysis, RoHR analysis, mass fraction burned (MFB) analysis, and knock and noise analysis.

Pressure-Crank Angle Analysis. In-cylinder pressure data analysis is an effective tool to analyze engine combustion. It directly influences engine power output, combustion, and emission characteristics. In this study, in-cylinder pressure data was recorded on the basis of crank-angle position. In all crank angle basis results, before top dead center (bTDC) position was represented by negative CAD and after top dead center (aTDC) position was represented by positive CAD. In order to reduce the effect of cyclic variations, average cylinder pressure data of 250 consecutive engine cycles was used for further analyses. Figure 6 shows the in-cylinder pressure variation w.r.t. crank angle position for different λ for different test fuels. P–θ diagram provides valuable information about the SoC, RoPR, and maximum cylinder pressure.

In Fig. 6, auto-ignition is clearly observed for all test fuels at all loads. Slope of in-cylinder pressure curve is a measure of RoPR, which is directly governed by chemical kinetics of the charge. Separation of in-cylinder pressure curve w.r.t. motoring curve shows the SoC. For all test fuels, shifting of SoC toward bTDC for richer mixtures is observed. This is due to the presence of large fuel quantity, which promotes rapid auto-ignition of fuel–air mixture inside the combustion chamber. For $\lambda = 1.5$, combustion starts well before TDC (20 deg bTDC) with an exception of diesoline, which shows earlier SoC however at lower loads, diesel combustion starts relatively earlier. At relatively richer fuel–air mixtures (for $\lambda < 3$), knocking is observed for all test fuels. Diesoline and diesosene showed highest knocking tendency due to their lower cetane numbers and auto-ignition temperatures. For all test fuels, knocking tendency at $\lambda = 2.25$ was higher compared to other engine loads. It caused longer knocking duration and an average of 250 cycles shows diminishing knocking behavior. At all loads, diesohol showed retarded SoC due to its higher auto-ignition temperature and poor solubility of ethanol in mineral diesel [26,27]. At higher engine loads, effect of volatile gasoline and ethanol addition can be observed. In both cases, improved combustion was also observed.

RoHR Analysis. RoHR analysis is an important parameter for characterizing HCCI combustion. HCCI heat release pattern is very different compared to conventional combustion modes [1,6]. RoHR of different test fuels in this study at different λ are shown in Fig. 7.

In HCCI combustion, higher RoHR is a major challenge for controlling combustion rates, which affects safety and structural

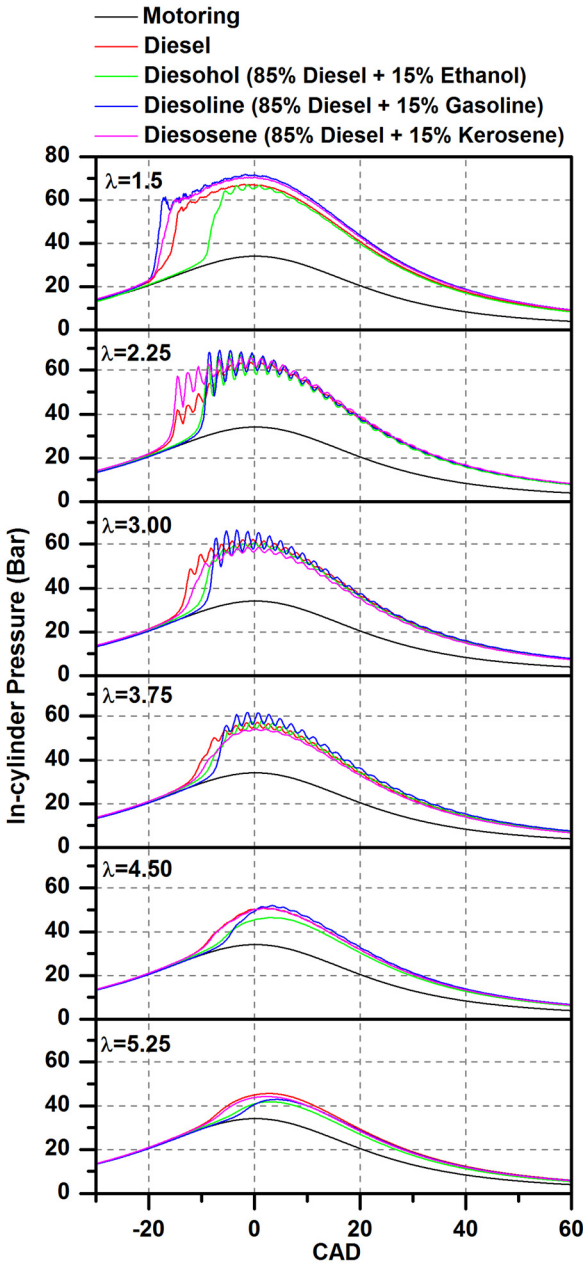

Fig. 6 In-cylinder pressure variation at different λ for constant intake air temperature and EGR

integrity of the test engine. Higher RoHR for richer mixtures in RoHR diagram is due to presence of larger fuel quantity, which enhances fuel–air mixture reactivity. At all loads, diesoline shows maximum RoHR, followed by diesosene. Higher calorific value and lower cetane number of gasoline are the most important factors responsible for this trend (Tables 3 and 4). Lower cetane number leads to higher ignition delay (except at $\lambda = 1.5$), which results in relatively longer premixed combustion duration compared to higher cetane number test fuels. At $\lambda = 1.5$, higher cetane number test fuels dominate over lower cetane number of gasoline resulting in relatively earlier SoC. Lower boiling temperature/range of gasoline and kerosene is responsible for this behavior, which enhances fuel volatility hence improves mixture homogenienty. At higher loads, earlier SoC of diesosene can also be seen in RoHR diagrams.

Figure 8 shows that the maximum in-cylinder pressure and maximum RoPR are relatively higher for diesoline. It was due to relatively higher calorific value and faster combustion chemistry

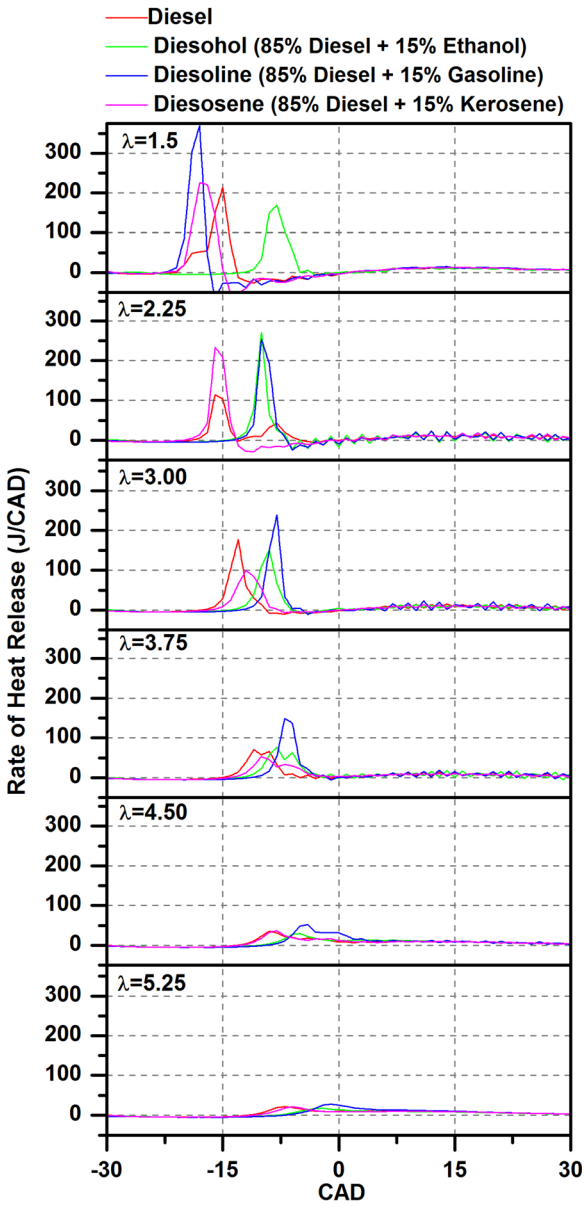

Fig. 7 RoHR at different λ for constant intake air temperature and EGR

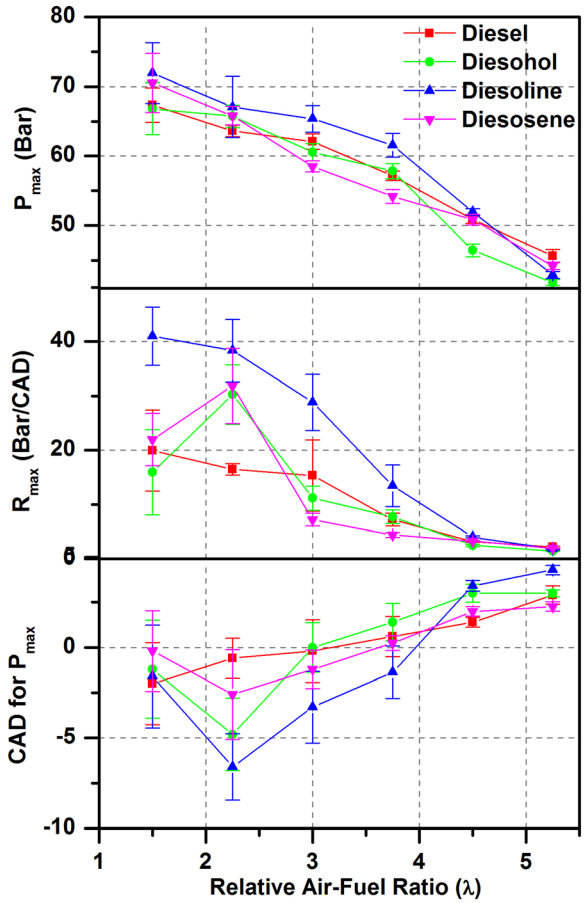

Fig. 8 Maximum in-cylinder pressure, maximum RoPR and position of maximum in-cylinder pressure at different relative fuel–air ratios for constant intake air temperature and EGR

of diesoline, which resulted in higher heat release rate peak compared to other test fuels (Fig. 7). For all test fuels, maximum in-cylinder pressure decreased with increasing λ, because injected fuel quantity reduced. The RoPR also increased with increasing load (i.e., decreasing λ). At lower engine load (higher λ), maximum in-cylinder pressure and maximum RoPR of baseline diesel were higher compared to diesohol and diesosene. Lower cetane number of kerosene causes slower combustion of these fuels, and shortens the premixed combustion phase. Presence of ethanol not only increased RoHR of diesohol, but also retarded the SoC, as an effect of its lower cetane number. Maximum cylinder pressure position is another important parameter, which gives qualitative information about combustion phasing in HCCI combustion. For richer fuel–air mixtures, earlier P_{max} position was detected for diesoline and diesosene, however, this difference reduced with increased λ. Main reason for variation in maximum in-cylinder position was the presence of more volatile fuel components (such as gasoline, ethanol, and kerosene), which were present in lower quantity in the combustion chamber at lower loads. Diesohol resulted in relatively retarded peak pressure position compared to other test fuels due to evaporation of moisture traces present in diesohol, which has minor cooling effect.

MFB Analysis. Figure 9 shows MFB parameters. Ten percent MFB is considered to be SoC, 50% MFB is considered for combustion phasing and combustion duration is considered as the difference between 90% MFB and 10% MFB in CADs. Combustion duration is a measure of overall combustion rate, i.e., how fast or slow combustion process takes place in an engine cycle.

Figure 9 shows the effect of different volatile additives on SoC. For all test fuels, SoC retarded as mixture became leaner. It happened mainly due to lower mixture reactivity in lean conditions; therefore, it took longer time to start the combustion, thus, retarded CA_{10} timings. At lower engine loads (higher λ), SoC of diesel and diesosene was relatively earlier compared to diesoline and diesohol. Relatively higher cetane number of mineral diesel and lower auto-ignition temperature of kerosene were the reasons for this behavior. At higher engine loads (lower λ), different combustion behavior was observed due to dominating nature of these volatile fuel additives. Diesohol showed retarded SoC compared to other test fuels. Presence of moisture traces in diesohol reduces the reactivity of diesohol slightly, resulting in retarded SoC. Ethanol is unlikely to auto-ignite under standard CI conditions, due to its lower octane number. This is the main reason for retarded SoC of diesohol compared to other test fuels. Figure 9 shows variations in combustion phasing (CA_{50}) for all test fuels at different engine loads. Combustion phasing affected HCCI combustion efficiency, which decreased for very advanced combustion phasing as well as very late combustion phasing. Combustion during very advanced combustion phasing led to faster RoHR, steeper pressure rise and higher peak combustion temperature. Heat loss from the walls and

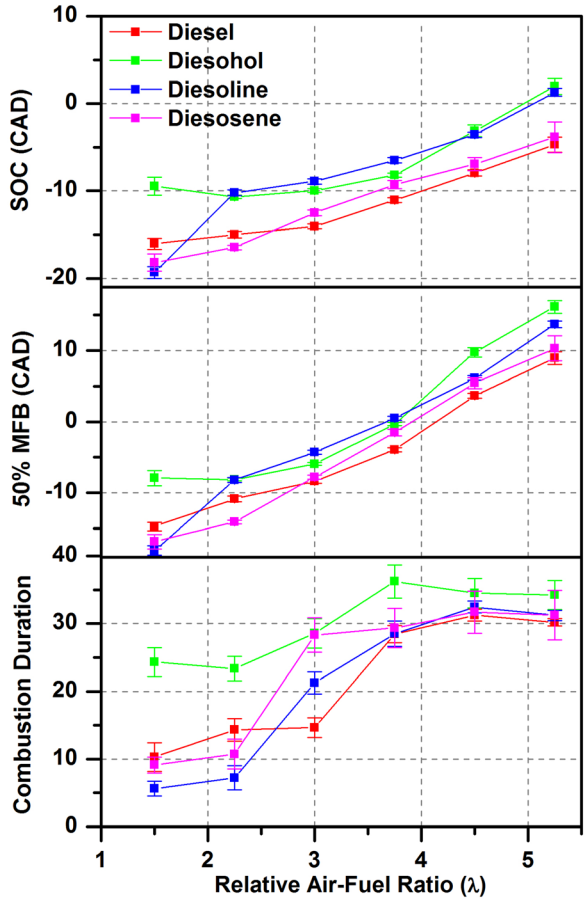

Fig. 9 SoC, 50% MFB and combustion duration at different relative fuel–air ratios for constant intake air temperature and EGR

piston increased and lower work was done on the piston by the expanding gases, leading to lower efficiency. In too retarded combustion phasing, combustion quality was inferior due to relatively lower peak combustion temperatures, which increased unburned HCs and CO emissions. Poor combustion efficiency resulted in lower thermal efficiency. Optimum combustion timing varied with engine load. Here optimum combustion phasing was observed for medium engine loads ($\lambda = 3$–4.5). All other combustion parameters also revalidated this λ range as optimized condition. Figure 9 shows that diesoline and diesel have better combustion phasing compared to diesohol and diesosene. At higher loads, combustion phasing for diesosene was advanced and diesohol was too retarded however at lower loads, retarded combustion phasing of both fuels (diesosene and diesohol) resulted in poor combustion efficiency of these fuels.

Comparison of combustion duration was done using MFB analysis because combustion duration affected both, the engine performance as well as combustion. Combustion duration was significantly affected by SoC and was higher for advanced SoC timings. Shorter combustion duration was typically observed in HCCI engine due to volumetric combustion of charge inside the combustion chamber. Relatively longer combustion duration was observed at $\lambda = 4.5$ and 5.25, which led to lower peak cylinder temperature. Combustion duration was also affected by fuel quantity injected and fuel–air mixture reactivity. At $\lambda = 3.75$ to $\lambda = 1.5$, combustion duration reduced drastically due to extremely high mixture reactivity, resulting in very fast combustion, which borders knocking combustion. Figure 9 shows that combustion duration of diesohol was relatively longer compared to other test fuels. Higher mixture reactivity of diesoline was due to higher volatility gasoline, which improved fuel–air mixing significantly compared to diesel and diesosene. Retarded SoC was the main reason for smaller combustion duration for diesohol.

Knock and Noise Analysis. Knocking and noise analysis was performed for determining knock integral and knock peak. Knock integral is the integral of the superimposed, rectified knock oscillations and knock peak reflects the absolute maxima of the rectified knock oscillations superimposed on cylinder pressure trace. For determining these knocking parameters, pressure signal is filtered through a high pass filter and then rectified. The parameters such as integral or peak value of the superimposed oscillations are determined from the measured signals. Noise level was also calculated from the cylinder pressure signals.

Figure 10 showed that maximum knock integral was observed for diesoline, followed by baseline mineral diesel. At lower loads, knock integral was lower and it increased with increasing engine load. This was due to presence of richer charge, which led to higher mixture reactivity. At $\lambda = 2.25$, knock integral was maximum due to excessive knocking, however, it reduced slightly for further richer mixtures. This result was similar to in-cylinder pressure results. Noise results followed similar trend as that of knock integral. At lower loads, noise level was less than 90 dB however for relatively richer mixtures, it reached levels, which are dangerous for human exposure. Maximum noise measured was 100 dB in case of diesoline. Noise and knock parameters are controlled by heat release during combustion, which is affected by fuel properties such as cetane number, fuel quantity, and combustion efficiency. When the fuel quantity injected was increased, RoPR during HCCI combustion also increased and resulted in an unacceptable noise (due to severity of detonation) which could potentially damage the engine, and lead to unacceptably high NOx

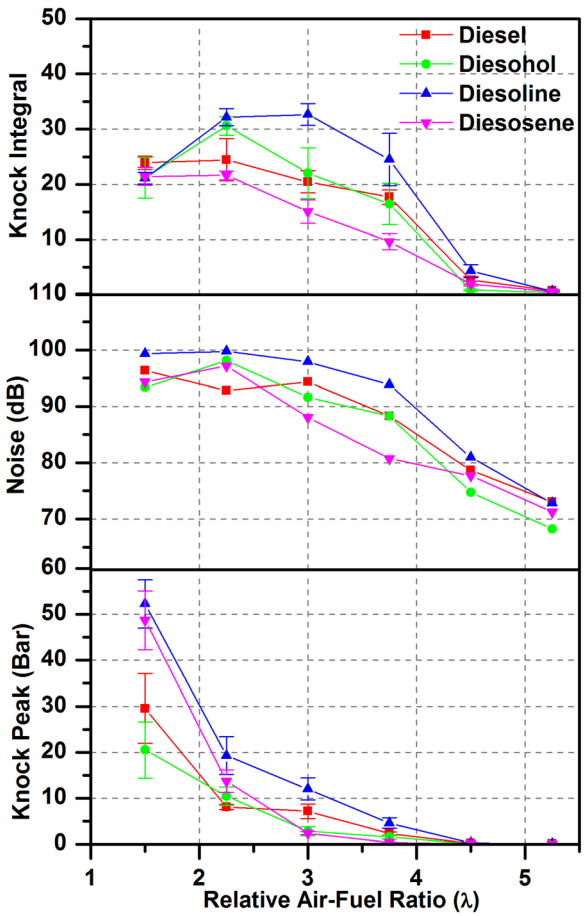

Fig. 10 Knock integral, noise and knock peak at different relative fuel–air ratios for constant intake air temperature and EGR

levels. At low loads (lower fuel quantity injected), HCCI RoPR decreased and combustion phasing was retarded, leading to reduction in cylinder pressure and temperature. For each test fuel, autoignition was dependent on cylinder pressure and temperature to start the chemical reactions. Therefore for late combustion phasing, noise and knock integral decreased. Knocking characteristics during CI occurred mainly due to ignition delay that caused a late shockwave inside the combustion chamber and produced noise. Ignition delay is controlled by fuel cetane number and higher cetane rating fuel gives smoother combustion as compared to lower cetane rating fuels. Knock integral and noise levels were the maximum for diesoline due to lower cetane number and superior combustion efficiency. Diesosene has higher cetane number (approx. 35) and poor combustion efficiency, which caused lower knock integral and noise. For diesel and diesohol, ignition delay and combustion efficiency were controlled by cetane number and moisture hence resulted in medium knock integral and noise level. Figure 10 also reflected knock peak for each test fuel. Knock peak mainly depends on RoHR. At higher engine loads, diesoline and diesosene showed higher RoHR, which resulted in higher knock peak compared to baseline diesel and diesohol. At medium loads, diesel dominated over diesosene and diesohol, however, knock peak moved toward zero for lower engine loads.

Performance Analysis. For the performance analysis of HCCI combustion, indicated thermal efficiency (ITE), indicated specific fuel consumption (ISFC), indicated specific energy consumption (ISEC), net IMEP, and EGT were calculated for each test fuel at all operating condition. This study was based on the in-cylinder combustion analysis (indicated parameters: net IMEP), hence, all performance parameters were compared in indicated reference condition.

EGT was measured separately in both cylinders, i.e., CI combustion mode and HCCI combustion mode cylinders. EGT gives qualitative information about the bulk temperature inside the combustion chamber. Figure 11 shows that HCCI combustion mode cylinder has significantly lower EGT compared to conventional CI combustion mode and this is the main reason for extremely low NOx emissions from HCCI combustion. In HCCI mode, Diesohol showed lowest EGT among all test fuels. These moisture traces in the fuel affect the reaction rates, leading to slightly inferior combustion efficiency hence lower heat release rate. Diesoline and diesosene have slightly higher EGT compared to baseline diesel due to relatively higher calorific value of these test fuels. At lower loads, EGT for all test fuels was almost equal due to lower reactivity of leaner charge. Figure 11 shows the variation of ITE for all test fuels at different engine loads. In HCCI engine, heat losses are expected to be relatively lower compared to conventional CI or SI mode because of its lower combustion temperature and shorter combustion duration. In addition, HCCI engine uses homogeneous charge, which does not generate soot during combustion, therefore, radiative losses are almost absent. Relatively lower heat losses compensate for the effect of lower in-cylinder temperature, thus resulting in ITE in HCCI mode comparable to conventional CI mode. For all test fuels, ITE increased with increasing engine load (upto medium loads) due to presence of richer mixtures. However, at higher engine loads, ITE decreased due to relatively earlier SoC (Fig. 9), resulting in higher pumping losses. Diesoline showed maximum ITE, followed by baseline diesel and combustion phasing was the most important factor for this behavior. Mineral diesel and diesoline had optimum combustion phasing however diesohol showed retarded combustion phasing and diesosene showed relatively advanced combustion phasing. Both cases adversely affected the combustion efficiency and ITE. At lower engine loads, diesohol showed sharp reduction in ITE due to dominating effect of moisture traces present in diesohol, which affected reaction rates.

Figure 11 shows that all test fuels have almost similar ISFC at higher engine loads; however at lower engine loads, diesohol and diesosene showed slightly higher ISFC compared to diesel and diesoline. Lower ITE of diesohol and diesosene was the reason for this trend. For all test fuels, minimum ISFC was seen at medium loads. Main reason for this trend was relatively higher increase in power output compared to increase in fuel consumption. ISEC for different test fuels was calculated and its trend was similar to that of ISFC. Net IMEP is the main performance parameter, which is affected by different combustion characteristics such as combustion phasing, combustion duration, etc. Figure 11 shows that diesoline exhibited maximum net IMEP, followed by baseline diesel. Optimum combustion phasing was the reason for this. At higher loads, diesosene and diesohol showed comparable net IMEP.

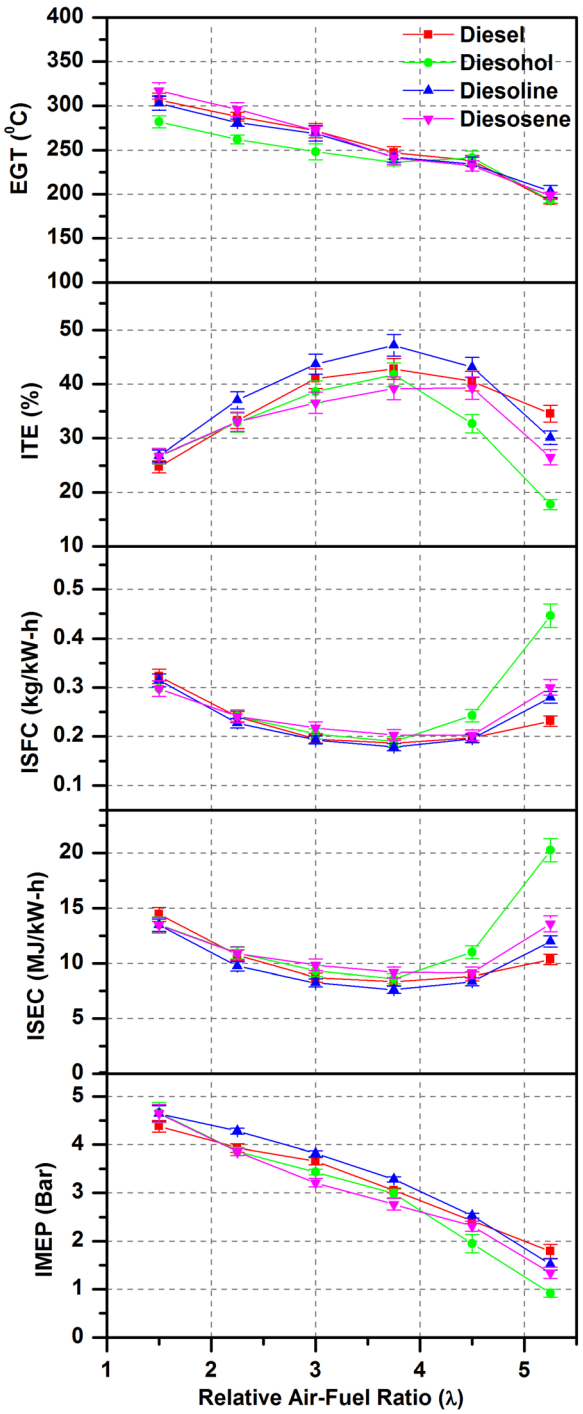

Fig. 11 Performance parameters at different relative fuel–air ratios for constant intake air temperature and EGR

At medium loads, diesosene showed lowest net IMEP. At lower engine loads, diesohol showed lowest net IMEP. Lower reaction rates of ethanol resulted in lower net IMEP from diesohol, however, inferior combustion efficiency of kerosene resulted in lower net IMEP for diesosene.

Exhaust Gas Emission Analysis. In this section, exhaust gas analysis for all test fuels at different test conditions was done and data was analyzed for mass emission of CO, HC, NO, and smoke opacity.

CO is a result of incomplete combustion of fuel in the combustion chamber. Retarded combustion phasing and incomplete combustion of leaner fuel–air mixtures resulted in higher CO emission from HCCI engine. Figure 12 shows that for all test fuels, CO emission followed similar trend and it increased with increasing λ. At lower engine loads, presence of lean fuel–air mixture resulted in relatively lower in-cylinder temperatures, which prevented oxidation of CO into CO_2. At higher loads, indicated specific carbon monoxide (ISCO) was almost similar for all test fuels however diesohol showed relatively higher ISCO at lower engine loads. It was due to reduced reactivity of alcohol in case of diesohol, that the power output was lower which resulted in higher ISCO. Moisture traces in diesohol absorbed some combustion generated heat, which resulted in relatively lower peak in-cylinder temperature, which reduced oxidation of CO into CO_2.

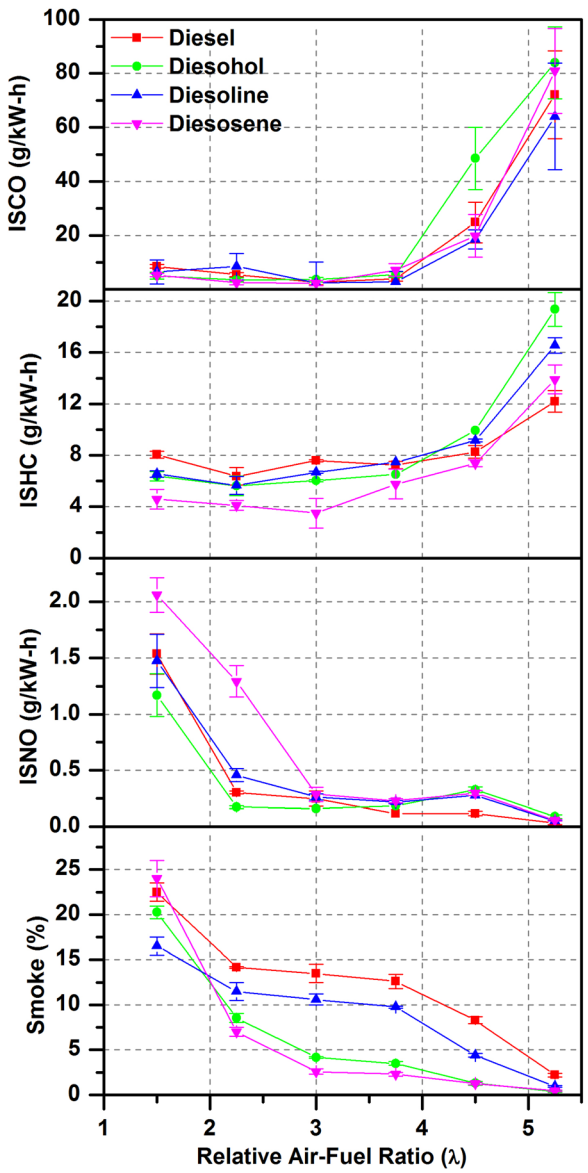

Fig. 12 Exhaust gas analysis at different λ for constant intake air temperature and EGR

Lower peak in-cylinder temperature in HCCI engine reduced NOx formation. However, the combustion temperature becomes too low to oxidize the fuel completely, thus resulting in higher unburned HC emission. Combustion temperature near the cylinder walls may be even lower due to higher heat losses. Combustion may be quenched and may not occur at all in the vicinity of cylinder walls. HC emissions in HCCI mode are generally high. Figure 12 shows the HC emissions from different test fuels. HC emissions increased with increasing λ. On increasing engine load, combustion chamber temperature increased. At higher engine loads, due to slightly inferior performance of the fuel vaporizer, some liquid fuel droplets enter the cylinder and move into crevice volume. During expansion stroke, they emerge in the combustion chamber along with exhaust and contribute to HC emissions. This is another reason for higher HC emissions from low volatility fuels in HCCI mode. At lower engine loads, diesohol showed highest HC emissions due to lowest in-cylinder temperature (Fig. 11) and retarded combustion phasing (Fig. 9).

Ultralow NOx emission is the main advantage of HCCI combustion. NOx formation is very sensitive to the peak combustion chamber temperature. NO emission is higher for richer mixture (lower λ) and vice versa closer to the misfire limit. From Fig. 12, it can be observed that NO formation increased drastically with increasing engine load. At higher engine load, combustion chamber temperature increased due to combustion of larger fuel quantity. NO formation also depends on combustion phasing because combustion chamber temperature increased with advanced combustion phasing due to earlier ignition and higher initial charge temperature, resulting in higher NO formation. At higher engine loads, diesosene emitted highest NO due to higher EGT (Fig. 11), due to enhanced volatility of fuel. Improved fuel vaporization led to advanced combustion phasing. Therefore, in-cylinder temperature increased and higher NO emission took place. Diesohol showed lower NO emission due to lower charge reactivity and reduces EGT (Fig. 11).

Low smoke opacity was another main advantage of HCCI combustion. Smoke is an indirect indicator of particulate in the exhaust. Significantly, lower smoke levels were observed for diesel and biodiesel HCCI combustion compared to CI combustion mode [15]. This was mainly due to combustion of homogeneous fuel–air mixture and absence of fuel-rich zones in HCCI mode, however, presence of fuel film on cylinder walls and other relatively cooler zones of the combustion chamber resulted in smoke formation, which is presented in this investigation. Figure 12 shows relatively lower smoke opacity in case of diesoline, diesosene and diesohol, compared to baseline mineral diesel. Relatively higher volatility of these test fuels compared to mineral diesel is the main reason for reduction in smoke opacity. Smoke opacity was higher in case of richer fuel–air mixtures due to relatively inferior vaporization of larger fuel quantity.

PAH Emissions. Although PAHs are unregulated pollutants, these species have severe environmental and human health impacts. PAHs are emitted in vapor form as well as they are adsorbed onto the surface of particulates. Figure 13(*a*) shows that the total PAH emission increased with increasing engine load (richer mixture). For leaner mixtures, diesosene and diesoline showed slightly higher PAH emissions and vice versa. Different combustion chemistry affected PAH formation, hence, combustion phasing is an important factor here. PAH emissions depend on engine load and fuel properties, leading to different combustion phasing. In most engine operating conditions, total PAH emissions were in the range of 50–500 ng/m^3. At very rich engine operating conditions, PAH emissions were in the range of 750–850 ng/m^3.

Figure 13(*b*) shows the percentage change in PAH emissions of different test fuels w.r.t. mineral diesel HCCI combustion.

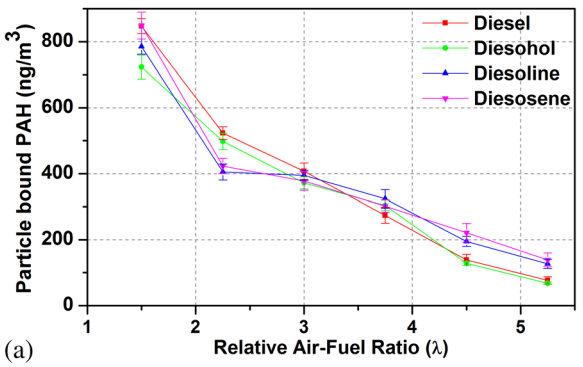

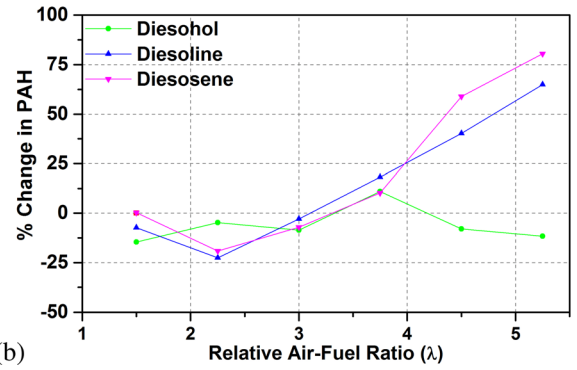

Fig. 13 (*a*) PAH emissions at different λ for constant intake air temperature and EGR and (*b*) percentage change in PAH emissions using different fuel blends w.r.t. baseline mineral diesel

At higher engine loads, PAH emissions reduced slightly from different volatile blends however at lower engine loads ($\lambda = 3.00$ to 5.25), PAH emissions from these blends increased. Diesohol showed slightly lower PAH emissions among all test fuels at most engine loads.

Particulate Emissions. This section describes particle number, surface area, and mass distributions w.r.t. particle size in order to characterize particulate emissions from HCCI combustion using the test fuels, i.e., diesoline, diesohol, and diesosene with respect to baseline mineral diesel. Particulate size-number distribution was determined after thermal stabilization of the engine. Particulate sampling was done for 1 min with a sampling frequency of 1 Hz. Average of these 60 data points for each engine operating condition using different test fuels was reported to minimize measurement errors.

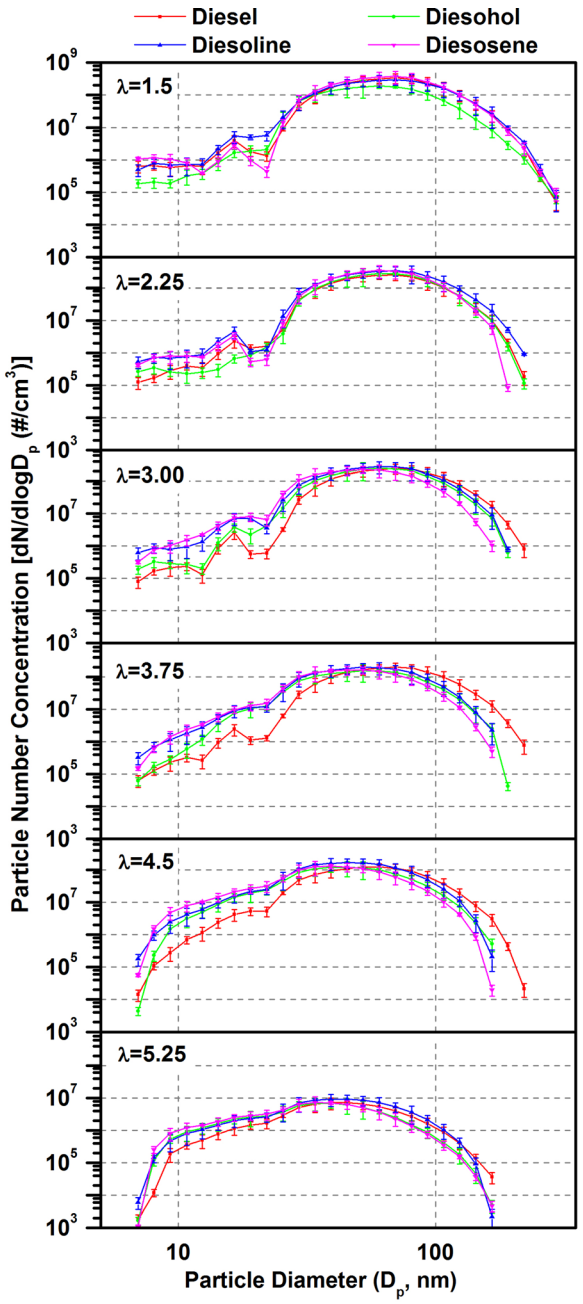

Fig. 14 Particle number-size distribution at different λ for constant intake air temperature and EGR

Particle Size-Number Distribution. Figure 14 shows that particle number distribution with size increased with increasing engine load for all test fuels. With increasing engine load, λ decreased. Fuel-rich conditions in HCCI mode favor soot formation and soot agglomeration. At lower engine loads, peak particle concentration was of the order of 10^7 particle/cm^3 however at higher engine loads, particle peak concentration increased upto 6×10^8 particle/cm^3. Nanoparticle concentrations were negligible at lower engine loads, however, it increased with increasing engine load. For each test fuel and load, peak of the particle concentration started from nanoparticle region ($D_p < 50$ nm) and ended in ultrafine region ($D_p > 50$ nm). Particle diameter corresponding to peak particle concentration increased with increasing load. Combustion of large fuel quantity leads to relatively richer homogeneous mixture combustion, which generated more gaseous and volatile species. These species condense on the particulates and increase their size. At all loads, diesosene showed maximum particles in nanorange and baseline mineral diesel emitted maximum particle concentration in ultrafine range. Diesohol showed minimum particle diameter for peak particle concentrations. Smaller molecular chain length of ethanol present in diesohol may be a possible reason for this trend. Minimum nanoparticle concentration was observed for mineral diesel, which was similar to the results reported by Agarwal et al. [15]. At lower loads, diesoline and diesohol showed slightly lower particle concentration, however at higher engine loads, diesoline showed slightly higher particle concentration compared to baseline diesel.

Figure 15(*a*) shows that total particle concentration increased with increasing load. This suggested that on increasing fueling (load), total particle concentration increased and the trend agreed with observations for HCCI combustion using diesel and gasoline [15,16]. For all test fuels, total number concentration was maximum at $\lambda = 1.5$ and varied from 6×10^8 particle/cm^3 to 8×10^8 particle/cm^3. Minimum total number concentration varied from

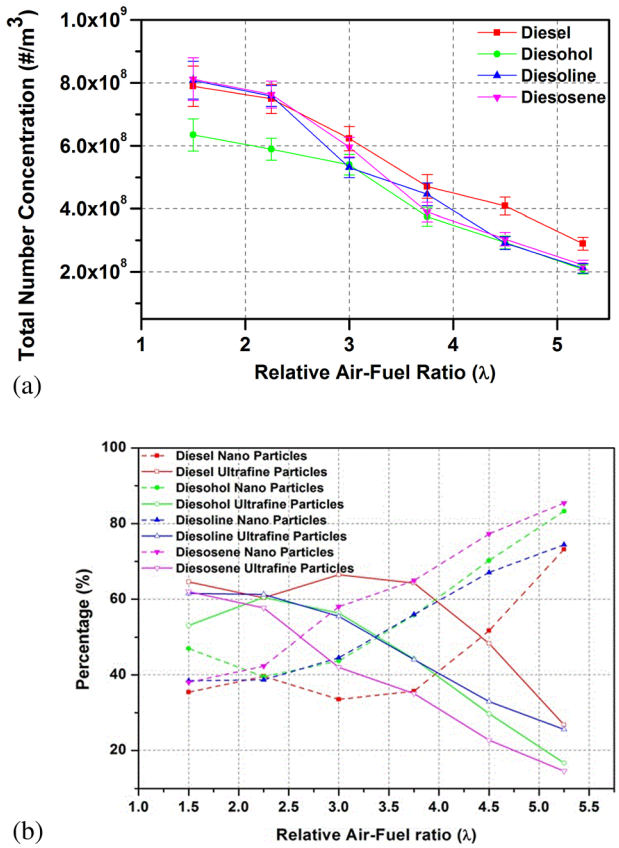

Fig. 15 Particle concentration at different λ for constant intake air temperature and EGR (*a*) total number concentration and (*b*) percentage contribution of nanoparticles and ultrafine particles in total number concentration of particles

2×10^8 particle/ cm^3 to 3×10^8 particles/ cm^3. Effect of volatile material addition was clearly observed in total particle concentration as diesoline and diesohol showed relatively lower total particle concentration compared to baseline mineral diesel. Due to inferior combustion efficiency at higher loads, slightly higher particle concentration was observed for diesosene compared to other test fuels. Figure 15(*b*) shows percentage contribution of nanoparticles and ultrafine particles in total particles emitted. Trends clearly showed that ultrafine particle concentration increased with increasing load due to presence of larger number of soot precursors. It was also validated by Fig. 13. Similarly, at lower loads, nanoparticle concentration increased rapidly compared to ultrafine particles.

Particle Size-Surface Area Distribution. Particle surface area is a measure of particulate toxicity. Higher the surface area, higher will be probability of surface adsorption of gaseous species and condensation of PAHs, making these particulate more toxic. Particle surface area was calculated by assuming them to be spherical

$$dS = dN.(D_p)^2$$

Here, dS is the area concentration of the size range with mean diameter D_p and dN is the number concentration of particulates with mean diameter D_p. Smaller particles tend to have significantly higher surface area for the same particle mass compared to larger particle, thus offering larger surface area for condensation of toxic volatile organic components (VOC's) and PAHs. Therefore, smaller particles tend to become more hazardous for human health compared to larger particles.

Figure 16 shows that particle surface area increased with increasing engine load. For richer fuel–air mixtures, particle surface area reached upto$\sim 10^{13}$ nm^2/cm^3 however for leaner fuel–air mixtures, it was only upto $\sim 10^{11}$ nm^2/cm^3. Shifting of peak particle concentration toward ultrafine particles was the main reason for higher particle surface area at higher loads. Particle size-surface area distribution also shifted toward ultrafine range with increasing load. At lower loads, diesel showed maximum particle surface area due to higher particle concentration and bigger particle sizes compared to other test fuels. Similarly at higher engine loads, diesosene showed highest particle surface area distribution. This result indicates toward higher toxicity of kerosene–diesel blends as compared to other fuels in HCCI combustion mode.

Particle Size-Mass Distribution. Figure 17 shows the variation of particle size-mass distribution ($\mu g/m^3$ of exhaust gas) at different engine loads for these test fuels. Higher particle mass distribution increases the possibility of its settling down quickly because

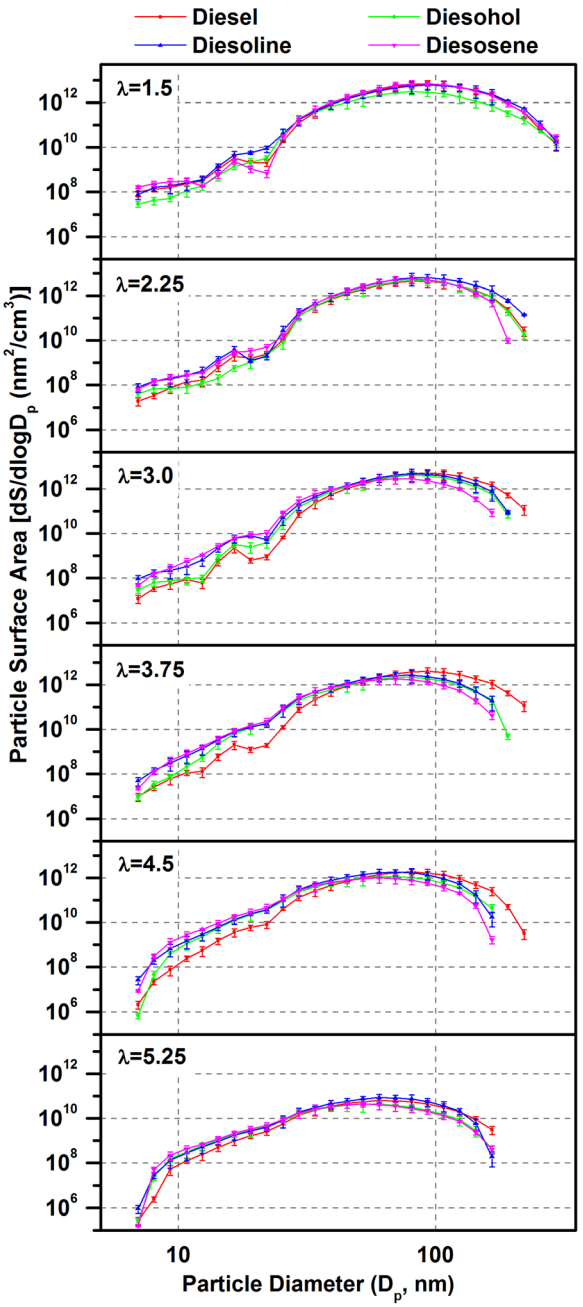

Fig. 16 Particle size-surface area distribution at different λ for constant intake air temperature and EGR

lighter particles have higher ambient retention time. Lighter particles are therefore more harmful compared to heavier particles. Constant particle density of 1.0 g/cm^3 was used in the calculations in this study. Higher particle mass distribution was observed for richer fuel–air mixtures due to large fuel quantity injected, which produced bigger and larger number of particulates. Particulate mass distribution for all test fuels varied from 10^3 to 10^5 μg/m^3. At lower loads, baseline mineral diesel showed higher particle mass distribution in the ultrafine particle range, however, diesosene showed slightly higher particle mass distribution for nanoparticles. At higher engine loads, particle mass was dominated by diesoline and baseline mineral diesel. Average particle mass was higher for mineral diesel, followed by diesoline and diesosene.

Figure 18 shows the particle mass distribution comparison in nano- and ultra-fine ranges. It clearly indicated that ultrafine particles contributed more in total particle mass compared to nanoparticles. Effect of addition of volatile fuels was also evident in the results because diesel ultrafine particulates were much higher in number compared to other test fuels. Nanoparticle mass distribution shows that diesosene emitted maximum particulate mass in nanorange, followed by diesoline.

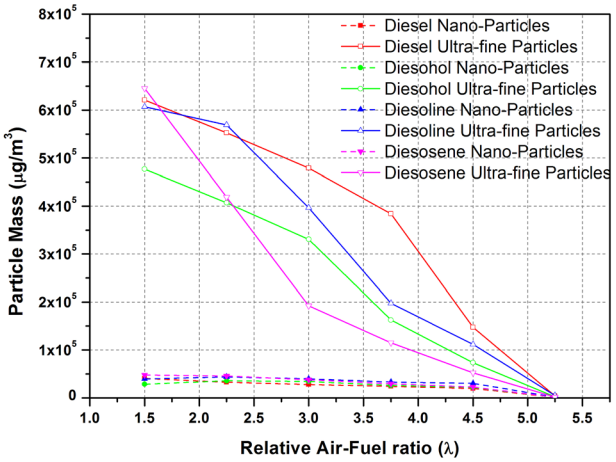

Fig. 18 Particle mass distribution in nanorange and ultrafine range for different λ at constant intake air temperature and EGR

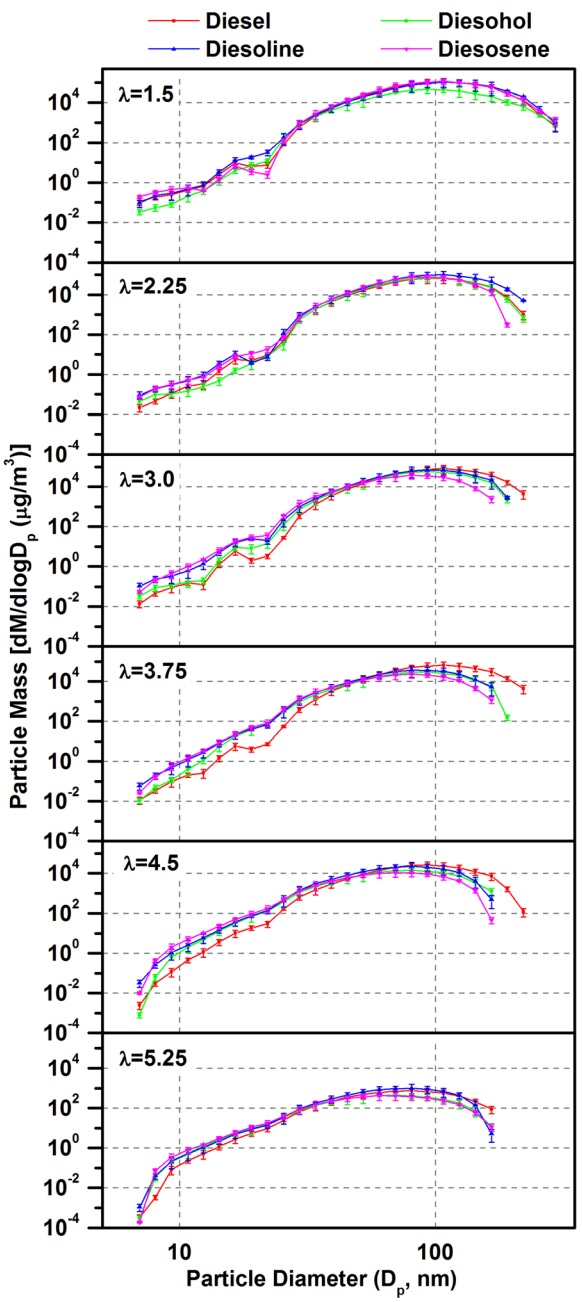

Fig. 17 Particle size-mass distribution at different λ for constant intake air temperature and EGR

Conclusions

Critical challenge in attaining diesel HCCI combustion is the low volatility of fuel. An attempt has been made to tackle this issue by adding volatile fuel additives in order to improve fuel's vaporization characteristics. In this study, HCCI combustion was investigated for three test fuels namely diesoline, diesohol, and diesosene vis-à-vis baseline mineral diesel. For homogeneous charge preparation, an external fuel vaporizer was used. In the experiments, additive effect on combustion phasing was found to be a key parameter, which affected HCCI engine's combustion, emissions and performance characteristics. Addition of gasoline and ethanol in diesel improved the combustion phasing, however, kerosene addition resulted in advanced combustion phasing. At lower loads, SoC and RoHR improved. Excessive knocking was observed at higher loads. This behavior was also validated by noise and knock analyses. Diesoline showed significant improvement in ITE and ISFC. Diesohol and diesosene delivered lower ITE and higher ISFC in HCCI mode, mainly due to lower reactivity of diesohol and relatively inferior combustion phasing of diesosene. Emission characteristics of HCCI combustion were significantly affected by volatile additives. HC and smoke emissions were relatively lower for diesoline, diesohol and diesosene compared to baseline diesel in HCCI mode. At $\lambda = 1.50$ to 3.00, PAH analysis showed slightly lower (approx. 10 to 100 ng/m^3) PAH's for all test fuels compared to baseline diesel. Particle characterization was carried out using EEPS. Slightly different particle size-number distribution was observed for all test fuels. At lower loads, diesel particle number concentration was higher in ultrafine range, however, it was slightly lower in nanoparticle range. Total particulate concentration was higher for mineral diesel compared to other test fuels. Results of particle size-surface area and size-mass distributions also supported addition of volatile additive to baseline diesel for improving HCCI combustion.

Finally, it can be concluded that addition of volatile additives such as gasoline, alcohols, and kerosene improved combustion, performance, exhaust emissions, and particle characteristics in HCCI combustion mode, especially upto medium loads.

Acknowledgment

Authors are thankful to Technology Systems Group, Department of Science and Technology (DST), Government of India for

providing financial support (Grant No. DST/TSG/AF/2011/144-G dated 14-01-2013) for undertaking this study. Grant from Council for Scientific and Industrial Research (CSIR), Government of India's SRA Scheme to Mr. Akhilendra Pratap Singh is also acknowledged, which supported his stay at ERL, IIT Kanpur for conducting the study.

Nomenclature

aTDC = after top dead center
bTDC = before top dead center
CA_{10} = crank angle for 10% mass fraction burned
CHR = cumulative heat release
CI = compression ignition
CO = carbon monoxide
CO_2 = carbon dioxide
DAQ = data acquisition system
dB = decibel
DI = direct injection
EEPS = engine exhaust particle sizer
EGR = exhaust gas recirculation
EGT = exhaust gas temperature
HC = hydrocarbon
HCCI = homogeneous charge compression ignition
IMEP = indicated mean effective pressure
ISCO = indicated specific carbon monoxide
ISEC = indicated specific energy consumption
ISFC = indicated specific fuel consumption
ISHC = indicated specific hydrocarbons
ISNO = indicated specific nitrogen oxide
ITE = indicated thermal efficiency
MFB = mass fraction burned
NO = nitrogen oxide
NOx = oxides of nitrogen
NVO = negative valve overlap
O_2 = oxygen
PAH = polycyclic aromatic hydrocarbons
PID = proportional integral differential
PM = particulate matter
RoHR = rate of heat release
RoPR = rate of pressure rise
SI = spark ignition
SoC = start of combustion
TDC = top dead center
VOC = volatile organic components

References

[1] Singh, G., Singh, A. P., and Agarwal, A. K., 2014, "Experimental Investigations of Combustion, Performance, and Emission Characterization of Biodiesel Fuelled HCCI Engine Using External Mixture Formation Technique," Sustainable Energy Technol. Assess., **6**, pp. 116–128.
[2] Yamada, H., Suzaki, K., Sakanashi, H., Choi, N., Choi, N., and Tezaki, A., 2005, "Kinetic Measurements in Homogeneous Charge Compression of Dimethylether: Role of Intermediate Formaldehyde Controlling Chain Branching in the Low-Temperature Oxidation Mechanism," Combust. Flame, **140**(1–2), pp. 24–33.
[3] Flowers, D., Aceves, S., Westbrook, C. K., Smith, J. R., and Dibble, R., 2000, "Detailed Chemical Kinetic Simulation of Natural Gas HCCI Combustion: Gas Composition Effects and Investigation of Control Strategies," ASME J. Eng. Gas Turbines Power, **123**(2), pp. 433–439.
[4] Aoyama, T., Hattori, Y., Mizuta, J., and Sato, Y., 1996, "An Experimental Study on Premixed Charge Compression Ignition Gasoline Engine," SAE Technical Paper No. 960081.
[5] Mancaruso, E., and Vaglieco, B. M., 2010, "Optical Investigation of the Combustion Behavior Inside the Engine Operating in HCCI Mode and Using Alternative Diesel Fuel," Exp. Therm. Fluid Sci., **34**(3), pp. 346–351.
[6] Singh, A. P., and Agarwal, A. K., 2012, "Combustion Characteristics of Diesel HCCI Engine: An Experimental Investigation Using External Mixture Formation Technique," Appl. Energy, **99**, pp. 116–125.
[7] Onishi, S., Jo, S. H., Shoda, K., Jo, P. D., and Kato, S., 1979, "Active Thermo-Atmosphere Combustion (ATAC)—A New Combustion Process for Internal Combustion Engines," SAE Technical Paper No. 790501.
[8] Najt, P. M., and Foster, D. E., 1983, "Compression-Ignited Homogeneous Charge Combustion," SAE Technical Paper No. 830264.
[9] Yao, M., Zheng, Z., and Liu, H., 2009, "Progress and Recent Trends in Homogeneous Charge Compression Ignition (HCCI) Engines," Prog. Energy Combust. Sci., **35**(5), pp. 398–437.
[10] Ryan, T., and Callahan, T., 1996, "Homogeneous Charge Compression Ignition of Diesel Fuel," SAE Technical Paper No. 961160.
[11] Dec, J. E., and Kelly-Zion, P. L., 2000, "The Effects of Injection Timing and Diluents Addition on Late-Combustion Soot Burnout in a DI Diesel Engine Based on Simultaneous 2D Imaging of OH and Soot," SAE Technical Paper No. 2000-01-0238.
[12] Shawn, M. M., Yann, G., and Giorgio, R., 2003, "Mixed-Mode Diesel HCCI With External Mixture Formation," Diesel Engine Emissions Reduction (DEER 2003), Newport, RI, Aug. 24–28.
[13] Ganesh, D., and Nagarajan, G., 2009, "Homogeneous Charge Compression Ignition (HCCI) Combustion of Diesel Fuel With External Mixture Formation," SAE Technical Paper No. 2009-01-0924.
[14] Kittelson, D. B., and Franklin, L., 2010, "Nanoparticle Emissions From an Ethanol Fuelled HCCI Engine," Cambridge Particle Meeting 2010, Minneapolis, MN, May 21.
[15] Agarwal, A. K., Lukose, J., Singh, A. P., and Gupta, T., 2013, "Characterization of Exhaust Particulates From Diesel Fuelled Homogenous Charge Compression Ignition Combustion Engine," J. Aerosol Sci., **58**, pp. 71–85.
[16] Agarwal, A. K., Gupta, T., Lukose, J., and Singh, A. P., 2015, "Particulate Characterization and Size Distribution of Gasoline Homogeneous Charge Compression Ignition Engine," Aerosol Air Qual. Res., **15**(2), pp. 504–516.
[17] Chao, Y., Jian-xin, W., Zhi, W., and Shi-jin, S., 2013, "Comparative Study on Gasoline Homogeneous Charge Induced Ignition (HCII) by Diesel and Gasoline/Diesel Blend Fuels (GDBF) Combustion," Fuel, **106**, pp. 470–477.
[18] Han, D., Andrew, M. I., and Stanislav, V. B., 2011, "Premixed Low-Temperature Combustion of Blends of Diesel and Gasoline in a High Speed Compression Ignition Engine," Proc. Combust. Inst., **33**(2), pp. 3039–3046.
[19] Tongroon, M., and Zhao, H., 2010, "Combustion Characteristics of CAI Combustion With Alcohol Fuels," SAE Technical Paper No. 2010-01-0843.
[20] Petrovic, V. S., Jankovic, S. P., Tomic, M. V., Jovanovich, Z. S., and Knezevic, D. M., 2011, "The Possibilities for Measurement and Characterization of Diesel Engine Fine Particles—A Review," Therm. Sci., **15**(4), pp. 915–938.
[21] Saxena, S., Schneider, S., Aceves, S., and Dibble, R., 2012, "Wet Ethanol in HCCI Engines With Exhaust Heat Recovery to Improve the Energy Balance of Ethanol Fuels," Appl. Energy, **98**, pp. 448–457.
[22] Saxena, S., Vuilleumier, D., Kozarac, D., Krieck, M., Dibble, R., and Aceves, S., 2014, "Optimal Operating Conditions for Wet Ethanol in a HCCI Engine Using Exhaust Gas Heat Recovery," Appl. Energy, **116**, pp. 269–277.
[23] Macka, J. H., Aceves, S. M., and Dibble, R. W., 2009, "Demonstrating Direct Use of Wet Ethanol in a Homogeneous Charge Compression Ignition (HCCI) Engine," Energy, **34**(6), pp. 782–787.
[24] Li, D. G., Zhen, H., Xingcai, L., Wu, Z., and Jian, Y., 2006, "Physico-Chemical Properties of Ethanol–Diesel Blend Fuel and Its Effect on Performance and Emissions of Diesel Engines," Renewable Energy, **30**(6), pp. 967–976.
[25] Mohammadi, A., Kee, S., Ishiyama, T., Kakuta, T., and Matsumoto, T., 2005, "Implementation of Ethanol Diesel Blend Fuels in PCCI Combustion," SAE Technical Paper No. 2005-01-3712.
[26] Ahmed, I., 2001, "Oxygenated Diesel: Emissions and Performance Characteristics of Ethanol–Diesel Blends in CI Engines," SAE Technical Paper No. 2001-01-2475.
[27] He, B. Q., Shuai, S. J., Wang, J. X., and He, H., 2013, "The Effect of Ethanol Blended Diesel Fuels on Emissions From a Diesel Engine," Atmos. Environ., **37**(35), pp. 4965–4971.
[28] Yadav, S., Murthy, K., Mishra, D., and Baral, B., 2005, "Estimation of Petrol and Diesel Adulteration With Kerosene and Assessment of Usefulness of Selected Automobile Fuel Quality Test Parameters," Int. J. Environ. Sci. Technol., **1**(4), pp. 253–258.
[29] Pathak, S., Aigal, A. K., Sharma, M. L., Narayanan, L., and Saxena, M., 2005, "Reduction of Exhaust Emissions in a Kerosene Operated Genset for Electrical Energy Applications," SAE Technical Paper No. 2005-26-026.
[30] Bergstrand, P., 2007, "Effects on Combustion by Using Kerosene or MK1 Diesel," SAE Technical Paper No. 2007-01-0002.